K-shell-ionization cross sections for low-Z elements ($11 \leq Z \leq 22$) by protons in the energy range 0.5–2.5 MeV

L. C. Tribedi and P. N. Tandon
Tata Institute of Fundamental Research, Homi Bhabha Road, Bombay 400 005, India
(Received 7 January 1992)

K-shell-ionization cross sections for Na, Mg, Al, Si, Cl, K, Ca, and Ti by protons in the energy range 0.5–2.5 MeV have been measured using thin targets. Measurements have also been performed for thin targets of Fe, Ni, and Cu at a few energies. The energy range of protons for these targets corresponds to the reduced velocity (v_1/v_{2K}) range 0.2–1.1, in which the cross sections are very sensitive to the increased binding energy and the Coulomb-deflection effects. The measured ionization cross sections are compared with the predictions of the theory based on the perturbed-stationary-state approach including the Coulomb-deflection, energy-loss, and relativistic corrections. The data have been scaled according to various scaling laws to test the validity of the universal nature of the various Coulomb ionization theories based on the plane-wave Born approximation, the binary-encounter approximation, and the simplified semiclassical approximation model as given by Lægsgaard, Andersen, and Lund [in *Proceedings of the Tenth International Conference on the Physics of Electronic and Atomic Collisions,* edited by G. Watel (North-Holland, Amsterdam, 1978), p. 353]. The measured data have also been compared with the calculations of Montenegro and Siguad [J. Phys. B **18**, 299 (1985)] based on the theory of $1s\sigma$ molecular-orbital ionization.

PACS number(s): 34.50.Fa, 34.70.+e

I. INTRODUCTION

Extensive measurements on the K-shell ionization of elements by proton and α-particle beams have been made in the past (see Ref. [1] for recent compilation). The measured ionization cross sections have contributed to the improvements in the Coulomb ionization theories using the plane-wave Born approximation (PWBA), binary-encounter approximation (BEA), and semiclassical approximation (SCA) with various corrective terms. The theoretical approach very commonly used is due to Brandt and Lapicki [2] and is referred to as the ECPSSR calculations. This calculation is based on the plane-wave Born approximation with hydrogenic wave function and corrected for energy loss of the projectile during the collision, deceleration, and deflection of the projectile in the Coulomb field of the target nuclei, the perturbation of the stationary target electron states by the passing projectile, and the relativistic electron motion. With the inclusion of these corrections the agreement between the experimental and the theoretical cross sections is quite good [1,3].

K-shell ionization cross sections are also required for elemental analysis using particle-induced x-ray emission technique (PIXE). An accurate knowledge of these cross sections is also very useful for the efficiency determination of the x-ray detectors, particularly in the low-energy region where it is difficult to obtain suitable radioactive sources. Paul and Muhr [4] have generated proton and α-particle-induced reference cross sections for all the elements from beryllium to uranium using the calculated ECPSSR cross sections and a large number of available experimental data. These cross sections are now being used with confidence for efficiency determination of x-ray detectors [5–7]. Unfortunately very few experimental data are available for the low-Z elements. An x-ray-production cross section for phosphorus has only recently been reported [8] along with sulfur, chlorine, and potassium while no data exist for $Z=11$ in the energy range investigated here [1,3]. Most numerous and most accurate x-ray-production cross sections are known for $21 \leq Z \leq 30$, which have also been included by Paul and Sacher [3] to calculate reference cross sections for low-Z elements down to $Z=11$. Clearly it is desirable to have x-ray-production cross-section data for low-Z elements in the energy range often used in PIXE. We report here proton-induced K-ionization cross-section measurements for Na, Mg, Al, Si, Cl, K, Ca, and Ti in the energy range 0.5–2.5 MeV and also for Fe, Ni, and Cu at a few energies. The cross sections were calculated from the measured K x-ray yield using thin targets.

We have compared the measured cross sections with the ECPSSR calculations, the BEA theory and the simplified SCA theory corrected for binding energy and Coulomb deflection effects as prescribed by Lægsgaard, Andersen, and Lund [9] (LAL) and Andersen, Lægsgaard, and Lund [10]. In addition to this we have also compared the data with the calculations of Montenegro and Sigaud (MS) based on the adiabatic perturbation theory for $1s\sigma$ molecular-orbital ionization [11]. Though the ECPSSR theory has been widely checked by many investigators, the validity of SCA-LAL model, in particular its universal nature, needs to be investigated in detail. In the present work, we have compared the scaled cross sections (using LAL prescription) with the universal SCA function for a wide range of reduced velocity ($0.2 < v_1/v_{2K} < 1.1$). Similarly, a detailed comparison of the experimental data with the MS model is also needed.

II. EXPERIMENTAL DETAILS

Thin targets of high-purity NaCl, Mg, Al, Si, KCl, Ca, Ti, Fe, Ni, and Cu were prepared by vacuum evaporation on self-supporting carbon foils of thickness 15–25 $\mu g/cm^2$. The thickness of each target is mentioned in Table I. These targets were mounted on a disc capable of accommodating 27 targets on two concentric circles. Each target could be brought into the path of the beam either manually or by remote control with the help of a stepper motor. The target holder assembly is mounted on an electrically isolated stainless-steel vacuum chamber having several ports for mounting x-ray and particle detectors. Another target holder, at a distance of 6 cm down stream from the center of the main target holder assembly, was used for mounting a gold foil for an independent beam current normalization. A fine collimated beam ($\simeq 1$ mm diameter) was allowed to pass through an electron suppressor before entering the chamber. It was stopped 30 cm away in a beam dump. The whole chamber, including the beam dump, was used for charge collection. Two silicon surface barrier detectors were mounted inside the chamber. One of them viewed the gold foil at an angle of 120°, and the other directly viewed the target at an angle of 135° with respect to the incoming beam. The Si(Li) x-ray detector was kept at 90° to the beam direction, in vacuum, inside the chamber at a distance of 95 mm from the target. The energy resolution of the detector was about 175 eV for the Mn $K\alpha$ line. Proton beams of energy varying between 0.5 to 2.5 MeV were provided by the Van de Graaff accelerator at Bhabha Atomic Research Center, Trombay. Molecular H_2 beam was used for energies below 1 MeV. The energy of the accelerator was calibrated using the threshold reaction $^7Li(p,n)$. The proton beam current was restricted such that in most of the cases the total count rate in the x-ray detector did not exceed 600 counts/sec in order to minimize the dead time and pile up corrections. The x-ray and the scattered particle spectra were recorded simultaneously on a multichannel analyzer.

The K-shell-ionization cross section $\sigma_{KI}(E_1)$ was obtained from the integrated counts under the K x-ray peak (Y_x) by using the relation,

$$\sigma_{KI}(E_1)=\frac{Y_x}{\epsilon(E)x\phi\omega_K}F(E,\Delta E_1)\ , \tag{1}$$

where ϕ is the number of incident particles with energy E_1, x the target thickness, $\epsilon(E)$ the absolute efficiency of the x-ray detector for a photon of energy E and ω_K the K-shell fluorescence yield for single vacancy as tabulated by Krause [12]. The factor $F(E,\Delta E_1)$ includes the corrections for the energy loss (ΔE_1) of the beam in the target and the self-absorption of the x-rays in the target material including the carbon backing. This correction

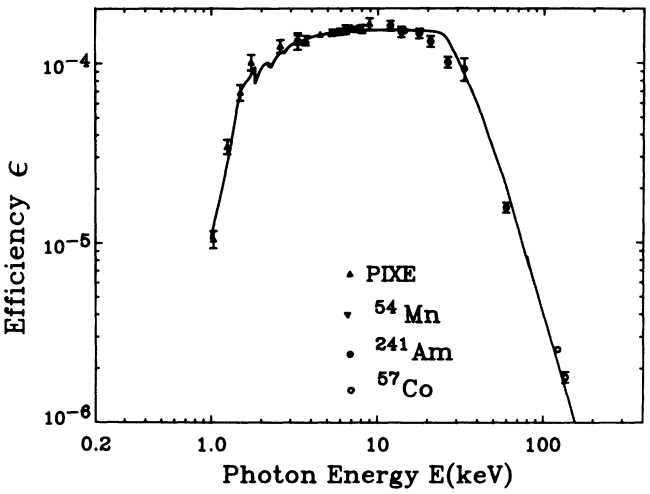

FIG. 1. Absolute efficiency as a function of photon energy for Si(Li) x-ray detector as obtained from standard radioactive sources and PIXE measurements. The solid line is the fitted efficiency curve.

was very small except for Na and Mg x-rays. The number of incident particles was obtained by collecting the charge from the entire chamber which was electrically isolated. The charge integration in each case was cross-checked by counting the elastically scattered particles from the gold foil. A low-energy proton beam (0.5–1.5 MeV) and an α-particle beam of energy 1–2 MeV were used to measure the thickness of various targets. In each case the elastically scattered particles from the specific element were counted and the target thickness obtained assuming pure Rutherford scattering. It should be mentioned here that for protons on low-Z elements, the nuclear resonance effect at large proton scattering angles makes the scattering cross section uncertain for some specific beam energies. In the present case the spread in the value of the target thickness thus derived using different charged particle beams of various energies was within 5–10% and was attributed to possible deviations [13] from Rutherford scattering. This normalization error, which can be viewed as an error in the target thickness measurement, is the main source of error for $Z \leq 14$. The absolute error in the cross sections quoted in Table II include this error.

The efficiency $\epsilon(E)$ for the detector was measured in the same geometry using well-calibrated, open-carrier-free radioactive sources of ^{54}Mn, ^{57}Co, and ^{241}Am which covered the energy range of 3.3–136 keV. The absolute efficiency at different energies was obtained using the known intensity of the emitted x-rays and γ rays [14] and is shown in Fig. 1. The data obtained in the overlapping energy region of 1–10 keV from the measured K x-ray

TABLE I. Thickness of the various targets in $\mu g/cm^2$.

Target	NaCl	Al	Si	KCl	Ca	Ti	Fe	Ni	Cu	Mg
Thickness	10.5	12.9	5.6	11.1	4.6	15.7	21.0	16.8	31.6	110

TABLE II. Proton-induced K-shell ionization cross sections. The measured K-shell-ionization cross sections (σ_{KI}) for various elements are given in column 3 for proton energies indicated in column 2. The errors in cross sections are shown in column 4. Columns 5 and 6 contain the cross sections (σ'_{KI}) measured by other researchers (obtained from the references as mentioned in the last column) and the corresponding errors, respectively. The quantity ω_k is the fluorescence yield.

Element ω_k	E (MeV)	σ_{KI} (b)	Error (b)	σ'_{KI} (b)	Error (b)	Reference
Na	0.5	2.50×10^4	0.5×10^4			
0.023	0.7	4.00×10^4	0.8×10^4			
	0.9	4.80×10^4	0.96×10^4			
	1.00	5.9×10^4	1.2×10^4			
	1.25	5.80×10^4	1.2×10^4			
	1.5	7.2×10^4	1.4×10^4			
	2.0	7.56×10^4	1.5×10^4			
	2.5	7.0×10^4	1.4×10^4			
Mg	0.5	9.70×10^3	1.94×10^3			
0.030	0.7	1.81×10^4	3.6×10^3	1.298×10^4	1.04×10^3	16
	0.9	2.34×10^4	4.6×10^3	2.210×10^4	1.77×10^3	16
	1.25	3.62×10^4	7.2×10^3			
	1.5	4.46×10^4	8.9×10^3			
	2.0	3.66×10^4	7.3×10^3			
	2.5	3.54×10^4	7.1×10^3			
Al	0.5	5.91×10^3	8.9×10^2	4.605×10^3	3.05×10^2	16
0.039	0.7	1.13×10^4	1.7×10^3	9.880×10^3	3.22×10^2	16
	0.9	1.60×10^4	2.4×10^3	1.489×10^4	9.80×10^2	16
	1.00	1.85×10^4	2.8×10^3	1.220×10^4	1.46×10^3	26
	1.25	2.19×10^4	3.3×10^3	1.580×10^4	1.90×10^3	26
	1.5	2.30×10^4	3.5×10^3	2.440×10^4	2.93×10^3	26
	2.0	3.36×10^4	5.0×10^3			
	2.5	2.94×10^4	4.4×10^3	2.430×10^4	2.92×10^3	26
Si	0.5	3.26×10^3	4.9×10^2			
0.050	0.7	6.48×10^3	9.7×10^2	5.53×10^3	4.40×10^2	16
	0.9	9.15×10^3	1.37×10^3	8.310×10^3	6.65×10^2	16
	1.00	1.21×10^4	1.8×10^3	1.09×10^4		13
	1.25	1.53×10^4	2.3×10^3			
	1.5	1.98×10^4	0.30×10^4	1.99×10^4	1.59×10^3	16
	2.0	2.23×10^4	0.33×10^4	1.83×10^4		13
	2.5	2.35×10^4	0.35×10^4			
Cl	0.5	592	59	4.45×10^2	3.5×10^1	16
0.097	0.7	1294	129			
	0.9	1873	187	1.480×10^3	1.2×10^2	16
	1.25	3640	364			
	1.5	4770	477			
	2.0	6244	624			
	2.5	7538	754			
K	0.5	163	16			
0.140	0.7	405	40			
	0.9	648	65			
	1.25	1365	136			
	1.5	1978	198			
	2.0	2773	277			
	2.5	4192	410			
Ca	0.5	88.6	9			
0.163	0.7	234	23	2.46×10^2	1.6×10^1	16
	0.9	473	47	4.76×10^2	3.1×10^1	16
	1.25	968	97			
	1.5	1375	137	1.39×10^3	1.0×10^2	16
	2.0	1992	199			
	2.5	2925	292			
Ti	0.5	34	2.7	36.9	2.7	16
0.214	0.7	92.6	7.4	98.2	6.9	16
	0.9	183	14	189	13	16

TABLE II. (*Continued*).

Element ω_k	E (MeV)	σ_{KI} (b)	Error (b)	σ'_{KI} (b)	Error (b)	Reference
	1.25	416	33			
	1.5	613	48	565	38	16
	2.0	951	76			
	2.5	1362	108			

yield with 1-MeV protons on various targets using the reference cross sections [3,4] are also shown in the same figure, and this data is in good agreement with the standard source data. It was fitted to the standard expression for efficiency [15], taking into account the silicon dead layer, Be window, the gold contact layer, and the active area of the detector as prescribed by the manufacturer.

III. RESULTS AND DISCUSSION

The values of $\sigma_{KI}(E_1)$ obtained for various elements are summarized in Table II and shown in Fig. 2 as a function of proton energy. The error includes the uncertainties in the target thickness (as described above), fluorescence yield [12], and the efficiency determination. The error in the efficiency was estimated to be $\simeq 10\,\%$ for <2 keV and about 6% above 2 keV. Table II also shows the recent data of other researchers wherever available [8,13,16]. The agreement between them is found to be quite good. The lines drawn through the points are the ECPSSR values for various energies as tabulated in Refs. [3] and [4]. In the following we compare the measured cross sections with various theoretical models. It is convenient to present all the data (for any target-projectile combination) in terms of the scaled cross sections in order to test the universality of the theory.

A. Binary encounter approximation (BEA)

In this model the K-shell-ionization cross section σ_K of an element with binding energy U_{2K} and atomic number Z_2 for a projectile with energy E_1 and charge Z_1 is given by

$$\sigma_{KI}^{\mathrm{BEA}}(E_1)=(N_K Z_1^2/U_{2K}^2)\sigma_0 G(V)\ , \tag{2}$$

where N_K is the number of electrons in the K shell, $V=v_1/v_{2K}$, v_1 and v_{2K} are the velocities of the projectile and the target electron in the K shell, respectively, $\sigma_0=6.56\times10^{-14}$ cm^{2}eV^2 and $G(V)$ is the universal BEA function depending only on the scaled velocity parameter V. In Fig. 3 we have plotted the reduced cross section

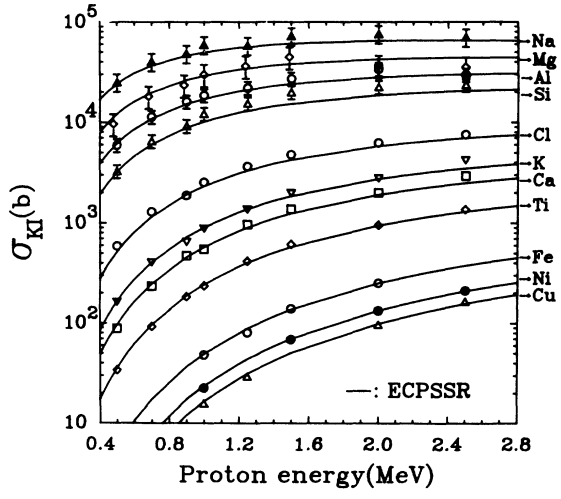

FIG. 2. K-shell-ionization cross sections (b) for Na, Mg, Al, Si, Cl, K, Ca, Ti, Fe, Ni, and Cu as a function of incident proton energy (MeV). The solid lines represent the ECPSSR values [3] for various elements as indicated in the figure.

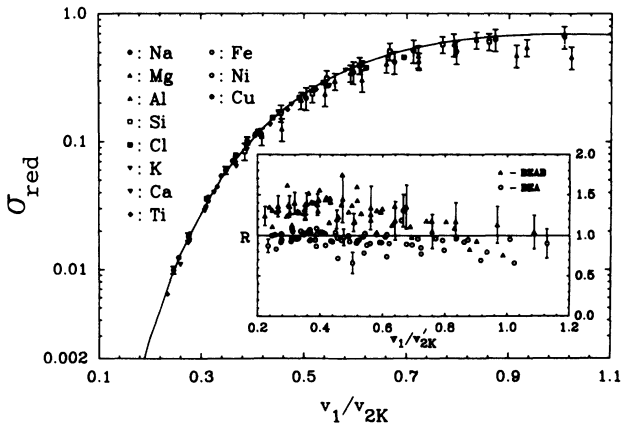

FIG. 3. Scaled cross sections ($\sigma_{\mathrm{red}}^{\mathrm{BEA}}$) [Eq. (3)] as a function of reduced velocity V. Typical errors (7–20 %) are shown at a few points. The solid line represents the universal BEA function $G(V)$. The inset shows the ratio $R=\sigma_{\mathrm{expt}}/\sigma_{\mathrm{theor}}$ for BEA (open circle) and BEAB (filled triangle). The variable along the x axis is v_1/v'_{2K}, where $v'_{2k}=v_{2k}$ for open circles and for closed circles v'_{2k} was calculated by using $\epsilon_K U_{2K}$ as the binding energy.

$$\sigma_{\rm red}^{\rm BEA}=\frac{\sigma_{\rm expt}U_{2K}^2}{N_K Z_1^2 \sigma_0} \tag{3}$$

as a function of V. The solid line denotes the universal function $G(V)$ taken from the calculations of Gerjuoy-Virens-Garcia as provided in Ref. [17]. The agreement between the experimental data and the theoretical values is good. The deviations from the theory are shown in the inset of this figure as the ratio $R=\sigma_{\rm expt}/\sigma_{\rm theor}$. It is seen from the figure that the theory explains the data quite well for $V\leq 0.6$ but overestimates it above 0.6. Including the correction due to increased binding energy the theory (BEAB) systematically underestimates the data by about 10–50 % for $V\leq 0.6$ above which it agrees with the measured data. This correction in the BEA was incorporated, as in PWBA, by replacing U_{2K} by $\varepsilon_K U_{2K}$, where ε_K is the *binding energy* correction factor defined by [18]

$$\varepsilon_K=1+\frac{2Z_1}{Z_{2K}\theta_K}g(\xi_K) \tag{4}$$

and the function $g(\xi_K)$ can be found in Ref. [18]. The reduced velocity variable ξ_K and the reduced binding energy θ_K are defined as:

$$\xi_K=2\left[\frac{\eta_K}{\theta_K^2}\right]^{1/2},$$

$$\eta_K=40.3\frac{E_1(\text{MeV})}{M_1(\text{amu})}\frac{1}{Z_{2K}^2},$$

$$\theta_K=U_{2K}/E_{2K}\ .$$

The parameter η_K is the reduced energy and $E_{2K}=Z_{2K}^2\mathcal{R}$, where $Z_{2K}=Z_2-0.3$.

B. Plane-wave Born approximation (PWBA)

It is known that the measured cross sections in the low-energy region are significantly less than the estimates based on PWBA. This deviation can be accounted for by including the increased binding energy and Coulomb-deflection effects [18]. At higher energy the deviations have been accounted for by introducing polarization corrections. Incorporating these corrections, the expression for ionization cross section is given by [19]

$$\sigma_K^{\rm BCP}=9E_{10}(\pi dq_0\xi_K)\left[\frac{\sigma_{0K}}{\zeta_K\theta_K}\right]F\left[\frac{\eta_K}{(\zeta_K\theta_K)^2}\right] \tag{5}$$

and the corresponding scaled cross section $\sigma_{\rm red}^{\rm BCP}$ can be written as

$$\sigma_{\rm red}^{\rm BCP}=\frac{\zeta_K\theta_K}{9E_{10}(\pi dq_0\zeta_K)}\left[\frac{\sigma_{\rm expt}}{\sigma_{0K}}\right], \tag{6}$$

where

$$\sigma_{0K}=8\pi a_0^2\left[\frac{Z_1^2}{Z_{2K}^4}\right]$$

and $9E_{10}(\pi dq_0\zeta_K)$ is the Coulomb-deflection factor. The quantity ζ_K takes care of the binding energy correction [i.e., ϵ_K in Eq. (4)] for low energy ($\xi_K\leq 1$) and polarization correction for higher energy ($\xi_K\geq 1$). These quantities were calculated using the expressions given in Ref. [19]. The quantity $q_0=U_{2K}/v_1$ is the minimum momentum transfer to the target K electron and d is the half-distance of the closest approach. Figure 4 shows the plot of the scaled cross section (PWBABCP) $\sigma_{\rm red}^{\rm BCP}$ along with the universal PWBA function $F(\eta_K/(\zeta_K\theta_K)^2)$ which is tabulated in Ref. [18]. It is seen from Fig. 4 that the agreement between the experimental data and the theoretical values is very good (see inset of Fig. 4).

C. Semiclassical approximation (SCA)

The semiclassical method as formulated by Bang and Hansten [20] is known to give a similar result as the PWBA. Lægsgaard, Andersen, and Lund [9] (LAL) have developed a simplified formulation of a semiclassical method that includes the binding energy and Coulomb-deflection corrections, maintaining the universal nature of the reduced cross section. Universality of the PWBABCP formulation has been thoroughly checked by many investigators (see Ref. [21] for a review) whereas the SCA-LAL formulation has been tested only for a few cases [7,13,22]. We have scaled our experimental data according to the prescription given by LAL [9,10] in the semiclassical approach (SCA-LAL) and compared it with the universal SCA function. This model leads to the following expression for the cross section:

$$\sigma_{KI}^{\rm LAL}=\frac{2^{12}\pi}{45}\frac{Z_1^2 r_K^2}{(U_{2K}/\mathcal{R})}F_1(\xi_K), \tag{7}$$

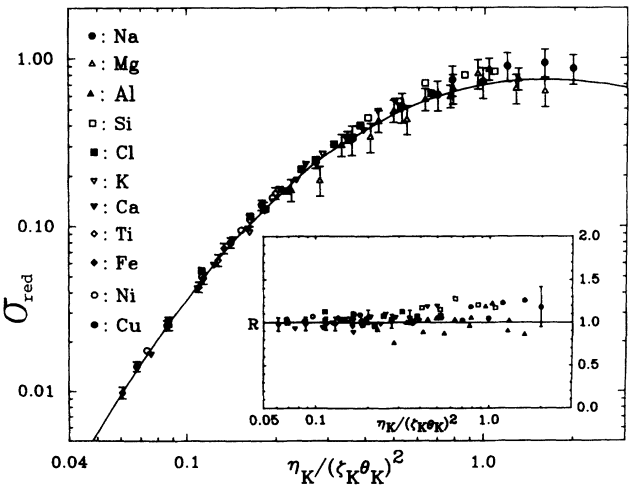

FIG. 4. Scaled cross sections ($\sigma_{\rm red}^{\rm BCP}$) in the PWBA formulation including the binding, Coulomb, and polarization corrections. The solid line is the universal PWBA function. Inset shows the deviation of the ratio $R=\sigma_{\rm expt}/\sigma_{KI}^{\rm BCP}$ from unity.

where $F_1(\xi_K)$ is the universal SCA function given by [9]

$$F_1(\xi_K)=\frac{\xi_K^8}{(1+0.0563\xi_K+1.38\xi_K^2+0.2191\xi_K^3)^4} \quad (8)$$

and $\mathcal{R}$ is the Rydberg constant. The experimentally measured cross sections can be scaled according to the SCA-LAL universal formula,

$$\sigma_{\rm red}^{\rm LAL}=\frac{45}{2^{12}\pi}\frac{\sigma_{\rm expt}(U_{2K}/\mathcal{R})}{Z_1^2 r_K^2} , \quad (9)$$

where $r_K=a_0/Z_{2K}$ is the K-shell radius of the target atom.

To describe the K-shell ionization in the low-velocity (adiabatic) region it is convenient to express ξ_K in the following manner:

$$\xi_K=r_{\rm ad}/r_K=q_K/q_0 , \quad (10)$$

where $r_{\rm ad}=hv_1/U_{2K}$ is the adiabatic distance and q_K the characteristic momentum of the target K-shell electron.

The reduced cross section using this formulation is found to be considerably lower than the theoretical values for $\xi_K<1$ and is more for $\xi_K\geq 1$ [see Fig. 5(a)]. This deviation from the simple model prediction has been explained and corrected by considering the effect of increased binding energy and Coulomb deflection. In the adiabatic limit ($\xi_K<1$) the general expression for the binding energy of the K-shell electron in the perturbed-stationary-state (PSS) approach can be written as [9,10]

$$U_{2K}=-\frac{e^2a_0}{2r_K'^2}+\frac{(Z_2-0.3)e^2}{r_K'}+\Delta U_{2K}(R,r_K')-\Delta E_{\rm screen} , \quad (11)$$

where ΔU_{2K} is the change in the electron binding energy due to the proximity of the projectile at a distance R from the target nucleus, and is given by [23]

$$\Delta U_{2K}=\frac{Z_1e^2}{R}[1-(1+R/r_K)\exp(-2R/r_K)] . \quad (12)$$

In the united-atom (UA) approximation prescribed by LAL, r_K' is chosen as the radius of the united atom ($r_K^{\rm UA}$) having atomic number (Z_1+Z_2), and the binding energy is obtained using Eq. (11) with $r_K'=r_K^{\rm UA}$. The Coulomb-deflection effect was viewed as the retardation of the projectile ion in the field of the target nucleus. Since ξ_K is a function of the binding energy and the projectile velocity [see Eq. (10)], it also gets modified whenever any correction is made in these parameters. The scaled cross section in this approximation is shown in Fig. 6. The solid line is the universal SCA function as given by Eq. (8). It is seen that SCA-LAL prediction for the scaled cross section is in good agreement with the universal curve $F_1(\xi_K)$ for $\xi_K\leq 1$. A similar agreement between the universal SCA function and the experimental data for heavier ions with $\xi_K<0.4$ is reported in Ref. [22]. Figure 5(b) shows the ratio R of $\sigma_{\rm expt}$ to $\sigma_{\rm theor}$ for this particular case. For $\xi_K>1$ the experimental data starts deviating from the theory, which is expected as according to the united-atom approximation the binding energy correction is appropriate only for $\xi_K\ll 1$.

A better agreement with the theory is obtained using the formalism given by Andersen, Lægsgaard, and Lund [10] (ALL) (see Fig. 7). In this method, unlike the united-atom model, the maximum binding energy (U_{2K}^m) is calculated at each ξ_K by varying r_K' numerically [using Eq. (11)]. The appropriate scaling of the cross section was done by using U_{2K}^m as the binding energy, r_K' as the radius, and the corresponding ξ_K (calculated from r_K' and

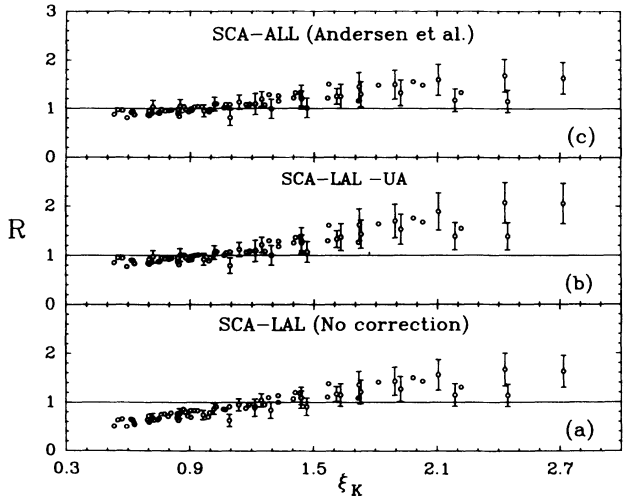

FIG. 5. The ratio $R=\sigma_{\rm expt}/\sigma_{KI}^{\rm LAL}$, (a) without any correction, (b) In the united-atom approximation, (c) the ratio $R=\sigma_{\rm expt}/\sigma_{KI}^{\rm ALL}$, where $\sigma_{KL}^{\rm ALL}$ was calculated from Eq. (7) by using U_{2K}^m as binding energy. U_{2K}^m was found, in each case, by maximizing the general expression of binding energy as given in Eq. (11). All the three ratios are plotted against the same reduced variable ξ_K obtained from Eq. (10).

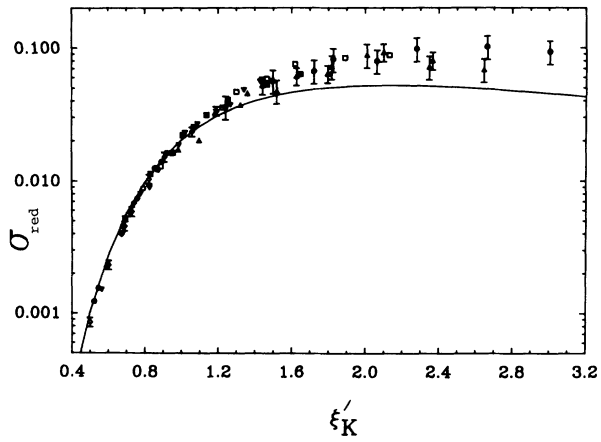

FIG. 6. The scaled cross sections $\sigma_{\rm red}^{\rm LAL\text{-}UA}$ vs ξ_K'. The reduced cross section $\sigma_{\rm red}^{\rm LAL\text{-}UA}$, was calculated from Eq. (9), by using $U_{2K}^{\rm UA}$ as the binding energy. The solid line is the universal SCA function given by Eq. (8). The variable along the x axis, i.e., ξ_K', was calculated from Eq. (10) using $U_{2K}^{\rm UA}$ as the binding energy and v_1 was corrected for Coulomb deflection [9]. Symbols have the same meaning as in Fig. 4.

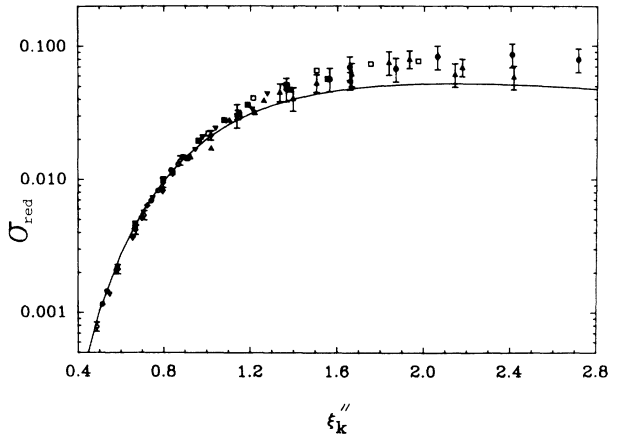

FIG. 7. The scaled cross sections σ_{red}^{ALL} vs ξ''_K. The reduced cross section σ_{red}^{ALL} was calculated from Eq. (9), by replacing U_{2K} as U_{2K}^m according to the SCA-ALL approach for binding energy correction [10]. The solid line is the universal SCA function given by Eq. (8). The variable along the x axis, i.e., ξ''_K, was calculated from Eq. (10) using U_{2K}^m as the binding energy and v_1 was corrected for Coulomb deflection [9]. Symbols have the same meaning as in Fig. 4.

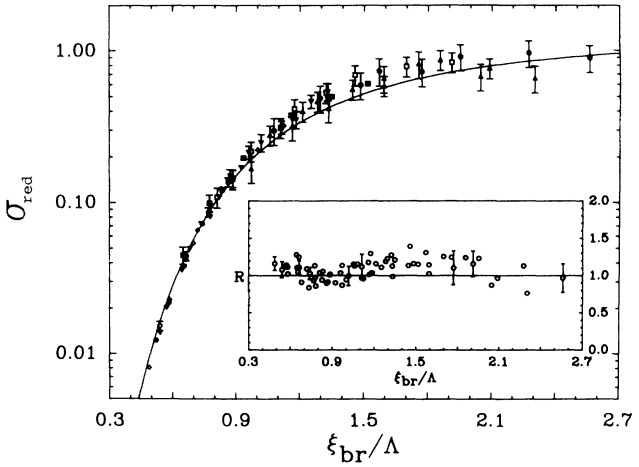

FIG. 8. The scaled cross sections (σ_{red}^{MS}) according to the MS model prediction obtained from Eq. (14). The universal function [Eq. (15)] is represented by the solid line. Symbols have the same meaning as in Fig. 4. The inset shows the ratio $R=\sigma_{expt}/\sigma^{1s\sigma}$.

U_{2K}^m). The corresponding ratio R between the experimental data and the theoretical values is plotted in Fig. 5(c). For $\xi_K > 1.4$ experimental points fall above the theoretical values. We feel that this could also be corrected by using polarization correction as in the case of PWBA formulation. For this the theory is to be modified to include the polarization factor. We have not included the relativistic corrections while scaling the cross sections.

D. Molecular orbital (MO) approach

Montenegro and Sigaud [11] (MS) have applied adiabatic perturbation theory, including the relativistic effects, to calculate the $1s\sigma$ molecular-orbital ionization in asymmetric ion-atom collision. This cross section is given by [11]

$$\sigma^{1s\sigma}=\Lambda^6[1+\gamma g(\xi_K)]^2 F_C \frac{\sigma_{0K}}{\bar{\theta}} F(\xi_{BR}/\Lambda) . \quad (13)$$

Accordingly the scaled cross sections can be expressed as

$$\sigma_{red}^{MS}=\frac{\sigma_{expt}^{1s\sigma}\bar{\theta}}{\Lambda^6[1+\gamma g(\xi_K)]^2 F_C \sigma_{0K}} , \quad (14)$$

where F_C is the Coulomb-deflection factor and $\bar{\theta}$ the reduced binding energy in the MS model and was calculated using the formulas given in Ref. [11]. The corresponding reduced velocity variable ξ_{BR} includes the relativistic effects. The quantity Λ is a function of Z_1, Z_2, and $g(\xi_K)$ and was calculated from the expression given in Ref. [11]. The universal function $F_2(\xi_{BR}/\Lambda)$ is given by [11,24]

$$F_2(x)=\frac{2^9}{45}\frac{x^8}{(1+1.72x^2)^4} . \quad (15)$$

The reduced cross sections include the relativistic corrections according to Brandt and Lapicki [25]. Figure 8 shows the reduced cross sections as given in Eq. (14) along with the universal function (solid line) $F(\xi_{BR}/\Lambda)$ plotted against the reduced variable ξ_{BR}/Λ.

The agreement between the experimental data and the theory over the entire energy range is reasonably good. Note that along with low (reduced) energy values the theory fits the data quite well for even higher energy values.

IV. CONCLUSION

K-shell-ionization cross sections of ten elements ($11 \le Z \le 30$) of Na, Mg, Al, Si, Cl, K, Ca, Ti, Fe, Ni, and Cu have been measured systematically for the incident proton beam of energy between 0.5–2.5 MeV using good-quality thin targets and a Si(Li) detector with accurately measured efficiency. The measured ionization cross sections in the present work will contribute to the data base for the inner-shell ionization in the low-Z region in which very little work has been performed. This data base is needed for a better understanding of the various mechanisms responsible for the inner-shell ionization phenomena. The absolute K x-ray production cross sections for the Na target are reported for the proton energy range investigated here. (We have recently seen work by Yu *et al.* [27], who have measured the K x-ray-production cross sections for low-Z elements, including Na, using proton beams. Their results for Na, Mg, and Al, in the energy range investigated here are in good agreement with our results.)

The measured data have been compared with most of the existing Coulomb ionization theories. The ionization cross sections obtained for all the elements and for all the energies coincide with the ECPSSR values as well as the reference cross sections [3] within experimental errors

(Fig. 2). The proton data can be described in the frame work of the BEA theory though the observed data points fall below predictions. The SCA formalism of Lægsgaard *et al.* (united atom) and Andersen *et al.* give good agreement with the data from the low-to-intermediate energy range ($0.2 \leq \xi_K \leq 1.4$). For higher energies the data deviate from the theories. The agreement between the measured cross sections and the MS model predictions for $1s\sigma$ molecular-orbital ionization is reasonably good. The PWBA theory including all the corrections (binding, Coulomb, and polarization) (PWBABCP) explains the data best over the entire energy range.

ACKNOWLEDGMENTS

The authors thank D. C. Ephraim for the preparation of targets, D. C. Karve, and M. B. Naik for their assistance in carrying out the experiment. They also thank the operators of the Van de Graaff for smooth operation of the machine.

[1] G. Lapicki, J. Phys. Chem. Ref. Data **18**, 111 (1989).
[2] W. Brandt and G. Lapicki, Phys. Rev. A **23**, 1717 (1981).
[3] H. Paul and J. Sacher, At. Data Nucl. Data Tables **42**, 106 (1989).
[4] H. Paul and J. Muhr, Phys. Rep. **135**, 47 (1986).
[5] N. A. Guardala, S. H. Greenberg, E. T. Williams, and D. Yan, Nucl. Instrum. Methods B **40/41**, 81 (1989).
[6] M. Pajek, A. P. Kobzev, R. Sandirk, R. A. Ilkhamov, and S. H. Khusmurodov, Nucl. Instrum. Methods B **42**, 346 (1982).
[7] M. Pajek, A. P. Kobzev, D. Trautmann, and Th. Kauer, Nucl. Instrum. Methods B **52**, 109 (1990).
[8] S. O. Olebanji and B. G. Martinsson, Nucl. Instrum. Methods B **24/25**, 81 (1987).
[9] E. Lægsgaard, J. U. Andersen, and M. Lund, in *Proceedings of the Tenth International Conference on the Physics of Electronic and Atomic Collisions,* edited by G. Watel (North-Holland, Amsterdam, 1978), p. 353.
[10] J. U. Andersen, E. Lægsgaard, and M. Lund, Nucl. Instrum. Methods **192**, 79 (1982).
[11] E. C. Montenegro and G. M. Sigaud, J. Phys. B **18**, 299 (1985).
[12] M. O. Krause, J. Phys. Chem. Ref. Data **8**, 307 (1979).
[13] M. Geretschläger, Ž. Šmit, and O. Benka, Phys. Rev. A **41**, 123 (1990), and references therein.
[14] K. M. Barfoot, I. V. Mitchell, L. Avaldi, H. L. Eschbach, and W. B. Gilboy, Nucl. Instrum. Methods B **5**, 534 (1984).
[15] J. H. Hansen, J. D. McGeorge, D. Nix, W. D. Schmidt-Ott, J. Uns, and R. W. Fink, Nucl. Instrum. Methods **106**, 365 (1973).
[16] I. Orlić, M. Budnar, V. Cindro, Ž. Šmit, and V. Valković, Nucl. Instrum. Methods B **40/41**, 108 (1989).
[17] J. H. McGuire and P. Richards, Phys. Rev. A **8**, 1374 (1973).
[18] G. Basbas, W. Brandt, and R. Laubert, Phys. Rev. A **7**, 983 (1973).
[19] G. Basbas, W. Brandt, and R. Laubert, Phys. Rev. A **17**, 1655 (1978).
[20] J. Bang and J. M. Hansteen, K. Dan. Vidensk. Selsk. Mat. Fys. Medd. **31**, No. 13, 1 (1959); J. M. Hansteen and O. P. Mosebekk, Z. Phys. **234**, 281 (1970); Nucl. Phys. **A201**, 541 (1973).
[21] T. J. Gray, in *Methods of Experimental Physics* edited by Patrick Richard (Academic, New York, 1980), Vol. 17, p. 193.
[22] Z. Żelazny and P. Hornshøj, J. Phys. B **17**, 1867 (1984).
[23] W. Brandt, R. Laubert, and I. Sellin, Phys. Lett. **21**, 518 (1966); Phys. Rev. **151**, 56 (1966).
[24] W. Brandt and G. Lapicki, Phys. Rev. A **10**, 474 (1974).
[25] W. Brandt and G. Lapicki, Phys. Rev. A **20**, 465 (1979).
[26] K. Sera, K. Ishii, M. Kamiya, A. Kuwako, and S. Morita, Phys. Rev. A **21**, 1412 (1980).
[27] Y. C. Yu, M. R. McNeir, D. L. Weathers, J. L. Duggan, F. D. McDaniel, and G. Lapicki, Phys. Rev. A **44**, 5702 (1991).